IV

Publication IV

T. Ojanen and T. T. Heikkilä, *State-dependent impedance of a strongly-coupled oscillator-qubit system*, Physical Review B **72**, 054502 (2005).

http://link.aps.org/abstract/prb/v72/p054502

State-dependent impedance of a strongly coupled oscillator-qubit system

Teemu Ojanen*
Low Temperature Laboratory, P.O. Box 2200, FIN-02015 HUT, Finland

Tero T. Heikkilä
Low Temperature Laboratory, P.O. Box 2200, FIN-02015 HUT, Finland and Department of Physics and Astronomy, University of Basel, Klingelbergstr. 82, CH-4056 Basel, Switzerland

(Received 21 December 2004; revised manuscript received 17 March 2005; published 1 August 2005)

We investigate the measurements of two-state quantum systems (qubits) at finite temperatures using a resonant harmonic oscillator as a quantum probe. The reduced density matrix and oscillator correlators are calculated by a scheme combining numerical methods with an analytical perturbation theory. Correlators provide us information about the system impedance, which depends on the qubit state. We show in detail how this property can be exploited in the qubit measurement.

DOI: 10.1103/PhysRevB.72.054502 PACS number(s): 42.50.Pq, 85.25.Cp, 03.67.Lx

I. INTRODUCTION

The growing interest in quantum information theory and the rapid development in nanotechnology have resulted in an extensive study of quantum two-state systems (qubits) and the quantum measurement theory. The measurement theory of frequency-independent detectors has been studied in detail in recent years.[1–4] Motivated by the new directions of research, we investigate possibilities to use a harmonic oscillator as a generic frequency dependent measuring device of a qubit.

Our system under study consists of a qubit coupled resonantly to a harmonic oscillator (Fig. 1), both coupled to a bosonic heat bath at a finite temperature. This model has a wide range of applications in solid-state physics as well as in quantum optics and has raised considerable attention lately.[5–12] In the literature, there exist various propositions to realize this system. In solid-state physics, the harmonic oscillator is realized by a resonator circuit and the qubit, for example, by a Josephson charge or flux qubit. The heat bath corresponds to the electromagnetic environment of the circuit. The connection of these systems to cavity QED has been explained and studied in Refs. 5 and 14.

Recently, also experimental studies of solid-state realizations of cavity QED have become accessible. Wallraff *et al.*[11] performed an experiment where they successfully managed to couple a transmission line resonator with a Cooper pair box acting as a qubit. They found a clear evidence of a quantum entanglement between the resonator and the qubit by measuring the vacuum Rabi mode splitting. Chiorescu and co-workers[10] realized the oscillator+qubit system by coupling a Josephson flux qubit to a superconducting quantum interference device (SQUID). In their experiment, the SQUID behaved like a harmonic oscillator and was used as a measuring device of the qubit. The entangled states of the oscillator-qubit system could be generated and controlled through the use of microwave spectroscopy. Very recently, Xu *et al.*[13] demonstrated controlled entanglement between a single LC oscillator and two Josephson phase qubits. The fact that the qubit is fixed on the same chip as the resonator allows circuit QED systems to explore the strong coupling regime of cavity QED, difficult to reach in quantum optics realizations.[9]

In the light of these recent experiments, we examine how the qubit information can be extracted from the oscillator measurement. Oscillator correlators reveal the entanglement between the qubit and the oscillator. The correlator information can be linked to experimentally accessible quantities. We propose a scheme to extract information about the state of the qubit by probing the impedance of the oscillator. This can be realized by a transmission measurement. As a result of such an experiment, one can resolve the diagonal state of the qubit. Such transmission measurements have been recently exploited in studying the solid-state cavity QED.[11]

Our paper is organized as follows. In Sec. II, we detail the general formalism for calculating the correlators and density matrices. We also explain the basics of the susceptibility measurement, and discuss the experimental realization of this measurement. In Sec. III, we study the susceptibility in various circumstances and how the state of the qubit can be read from the susceptibility information. Finally, we summarize and discuss the susceptibility measurement in Sec. IV.

II. GENERAL FORMALISM

Our starting point is a variant of the Jaynes–Cummings Hamiltonian, which describes a qubit coupled to a harmonic oscillator in the absence of dissipation:

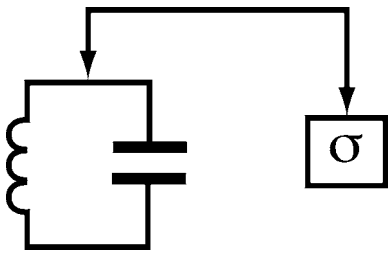

FIG. 1. Possible realization of the studied system. The resonator circuit is coupled to the qubit represented by σ. In practice, σ could be for example a Cooper-pair box with a capacitive coupling to the oscillator.

$$H_{\mathrm{JC}} = \hbar\omega_0 a^\dagger a - \frac{\hbar\omega_{\mathrm{qb}}}{2}\sigma_z + \frac{\hbar g}{2}\sigma_x(a + a^\dagger). \quad (1)$$

Operator σ/a operates on the qubit/oscillator degrees of freedom. The operators a and $a^\dagger$ obey the usual bosonic commutation relations. We assume the oscillator in resonance with the qubit, $\omega_0 = \omega_{\mathrm{qb}}$. In such a case, the excitation spectrum is doubly degenerate if oscillator-qubit coupling g vanishes. A finite coupling $g \ll \omega_0$ slightly lifts the degeneracy of the spectrum leading to the Rabi splitting. The properties of the spectrum of Eq. (1) are analyzed in detail in Ref. 14.

The total Hamiltonian under study is

$$H = H_{\mathrm{JC}} + H_B^{\mathrm{qb}} + H_B^{\mathrm{osc}} + H_{\mathrm{int}}^{\mathrm{qb}} + H_{\mathrm{int}}^{\mathrm{osc}}, \quad (2)$$

where $H_B^{\mathrm{qb}} = \Sigma_i \hbar\omega_i b_i^\dagger b_i$ and $H_B^{\mathrm{osc}} = \Sigma_j \hbar\omega_j c_i^\dagger c_i$ describe the environments of the qubit and the oscillator, respectively. In addition, $H_{\mathrm{int}}^{\mathrm{qb}} = \sigma_x \Sigma_i g_i (b_i + b_i^\dagger)$ and $H_{\mathrm{int}}^{\mathrm{osc}} = (a^\dagger + a)\Sigma_j g_j (c_j + c_j^\dagger)$ couple the system to the environment. The chosen bath model is a popular choice for its conceptual and technical simplicity.[15]

Our strategy is to calculate the reduced density matrix of the oscillator-qubit system and the oscillator correlators by numerically diagonalizing the qubit+oscillator system and taking the environment into account perturbatively. Only the lowest-order contributions of the perturbation series are assumed to be significant. However, to obtain a finite linewidth of energy levels of the oscillator+qubit system, the perturbation series must be analytically resummed to the infinite order.

A. Perturbation theory

We apply the perturbation theory for an open system, developed, for example, in Refs. 16, 17, and 19. The time evolution of the density matrix involves forward and backward propagators which get coupled after tracing out the environmental degrees of freedom. Given a complete set of energy eigenstates of a quantum system, the evolution of the density matrix can be expanded in this basis as

$$f_{n_1 n_2}(t) = \sum_{n'_1, n'_2} \Pi_{n_2 n'_2}^{n_1 n'_1}(t, t') f_{n'_1 n'_2}(t'), \quad (3)$$

where $\Pi_{n_2 n'_2}^{n_1 n'_1}(t, t')$ is the reduced propagator and $f_{n_1 n_2}(t')$ is the initial reduced density matrix. In the graphical language, the propagator is the sum of all Feynman diagrams with the given states at each end. The Feynman rules for an open system, particularly for a quadratic environment with a bilinear coupling term are described in Refs. 16 and 17.

Supposing that at the initial time the density matrix of the system+environment is of a tensor product form, the perturbation theory is significantly simplified. In the frequency space, the propagator is defined as

$$\Pi_{n_2 n'_2}^{n_1 n'_1}(\omega) = \int_0^\infty e^{i\omega(t-t')} \Pi_{n_2 n'_2}^{n_1 n'_1}(t, t') d(t - t'). \quad (4)$$

The full propagator is described by the Dyson equation

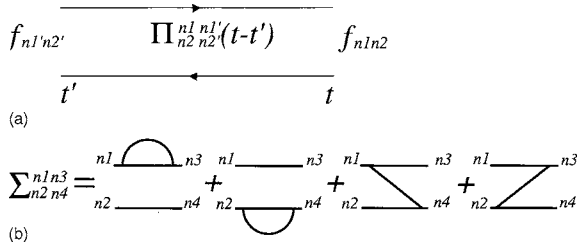

FIG. 2. (a) Propagator evolves the initial state specified by the density matrix $f_{n1'n2'}$. (b) Second-order contributions to the irreducible self-energy Σ.

$$\Pi_{n_2 n'_2}^{n_1 n'_1}(\omega) = \Pi^{0 n_1 n'_1}_{n_2 n'_2}(\omega) + \Pi_{n_2 r}^{n_1 s}(\omega)\Sigma_{rl}^{sp}(\omega)\Pi^{0 p n'_1}_{l\, n'_2}(\omega), \quad (5)$$

where $\Sigma_{rl}^{sp}(\omega)$ is the irreducible self-energy and $\Pi^{0 p n'_1}_{l\, n'_2}(\omega)$ is the free propagator. Summation over the repeated indices is implied. The free propagator elements are determined by the energy eigenvalues of the reduced system alone:

$$\Pi^{0 n_1 n'_1}_{n_2 n'_2}(\omega) = \frac{i}{(E_{n_2} - E_{n_1})/\hbar + \omega + i\eta}\delta_{n_1 n'_1}\delta_{n_2 n'_2}. \quad (6)$$

In our case, the energies in Eq. (6) are the exact energy eigenvalues of the oscillator+qubit system. The perturbation theory is needed only in taking the external baths into account. After calculating $\Sigma_{rl}^{sp}(\omega)$ to the desired order, the exact propagator can be solved from Eq. (5). In our work, we only take into account the second-order contributions to $\Sigma_{rl}^{sp}(\omega)$, see Fig. 2(b). This is the Born approximation. For example, the first of the self-energy diagrams represents the expression

$$\sum_n \int_{-\infty}^{\infty} \frac{J(\omega')f(\omega')d\omega'}{\omega + (E_{n2} - E_n)/\hbar + \omega' + i\eta}\langle n|x|n1\rangle\langle n3|x|n\rangle\delta_{n2n4},$$

where $J(\omega')$ is the spectral density of the bath and $f(\omega')$ is the Bose distribution function. The operator x corresponds to either $(a + a^\dagger)$ or σ_x depending on whether the diagram represents the oscillator or the qubit interacting with the bath. The spectral density is chosen to produce an ohmic damping. For both cases, it can be written as $J(\omega) = \mathrm{const} \times \omega$ below the cutoff frequency which is much larger than the characteristic frequency ω_0. The prefactor is different for the qubit-bath and the oscillator-bath interaction and determined by the quality factor of the oscillator and the qubit lifetime, respectively. For the oscillator-bath interaction, the prefactor is $\hbar/2Q = \hbar\pi\kappa/\omega_0$ and for the qubit-bath interaction $\hbar\pi\gamma/\omega_0$, where κ and γ are the inverse lifetimes of the resonator and the qubit.

Correlators $\langle A(t_2)B(t_1)\rangle$ contain important information about the system. Generally, they are functions of the two time variables t_1 and t_2, but in a steady state they depend only on the relative time $t_2 - t_1$ due to the temporal invariance. In this paper, we make use of a mixed representation where the correlators depend on one time variable $t = \min(t_1, t_2)$ and one frequency variable ω:

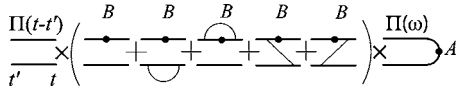

FIG. 3. Diagrammatic representation of the correlator (7). First, the initial state develops to the moment t, then follows external vertex B and the vertex corrections. The last step is the propagation in the frequency space to the other external vertex A.

$$D_{AB}(\omega,t)=\int_0^\infty e^{i\omega|t_2-t_1|}\langle A(t_2)B(t_1)\rangle d|t_2-t_1|. \tag{7}$$

If the system is in a steady state, $D_{AB}(\omega,t)$ is independent of t. The reason for considering correlators of the type $D_{AB}(\omega,t)$ is that in Sec. III we study the temporal evolution of the quasistatic susceptibility of the oscillator+qubit system.

Correlators cannot be calculated from the reduced propagator and the initial density matrix alone. The diagrammatic method of calculating correlators in an open system is presented in Refs. 18 and 19. To calculate the correlator (7), we first need to solve the temporal evolution of the reduced density matrix from the initial time t' to $t=t_1$ (assuming $t_1<t_2$). This task can be performed with the help of $\Pi^{n1n1'}_{n_2n2'}(t,t')$. Next, we have to calculate the vertex corrections in the first external vertex B, and propagate the system with $\Pi^{n1n1'}_{n_2n2'}(\omega)$ to the other vertex A. Correlator (7) is schematically illustrated in Fig. 3.

In the case when the system interacts weakly with the bath one further simplification occurs. The quantum regression theorem[20,21] allows one to calculate the correlator (7) with the propagator and the initial density matrix alone:

$$D_{AB}(\omega)=f^0_{n'_1n'_2}\Pi^{n_1m}_{n_2n'_2}(\omega)A_{n_1n_2}B_{mn'_1}. \tag{8}$$

In the diagrammatic language, this means that the vertex corrections in the external vertex B are negligible. This result can be applied when the second-order bath corrections provide an adequate description of the damping effects and the memory effects of the bath can be neglected.

B. Numerical scheme

For computing the propagator, the energy eigenvalues and eigenstates of the oscillator-qubit system are calculated numerically. This is done by taking into account only the N lowest energy eigenstates of the oscillator. The lower the temperature with respect to $\hbar\omega_0$, the less states N is needed. The propagator contains $16N^4$ terms. Fortunately, the interaction with the bath couples only states of the reduced system differing roughly by $\hbar\omega_0$ in energy.[14] For this reason, the effective number of propagator elements is proportional to N^2.

The reduced density matrix and correlators can now be computed from Eqs. (3) and (8) (see also Fig. 2).

C. Oscillator measurement

In studying the effects of the qubit on the oscillator we need to identify convenient measurable quantities. The idea is to analyze how, by measuring oscillator observables, we can extract information about the qubit. In a steady-state situation, the cavity susceptibility of cavity QED is defined as

$$\chi_x(\omega)=i\int_0^\infty e^{i\omega t}\langle[x(t),x(0)]\rangle dt, \tag{9}$$

where $x=(a+a^\dagger)$. The direct analogue of the x susceptibility (9) in solid-state applications is the ϕ-susceptibility of a resonator circuit. The resonator circuit is characterized by two parameters, the inductance L and the capacitance C. Defining $Z_b=\sqrt{L/C}$ and following the conventions of Refs. 22 and 23, the ϕ-susceptibility is

$$\chi(\omega)=\frac{i}{\hbar}\int_0^\infty e^{i\omega t}\langle[\phi(t),\phi(0)]\rangle dt, \tag{10}$$

where

$$\phi=\left(\frac{\hbar Z_b}{2}\right)^{\frac{1}{2}}(a+a^\dagger). \tag{11}$$

The conjugate of ϕ is the charge operator

$$q=i\left(\frac{\hbar}{2Z_b}\right)^{\frac{1}{2}}(a^\dagger-a). \tag{12}$$

According to the linear response theory, the ϕ-susceptibility is proportional to the impedance of the system, $Z(\omega)=i\omega\chi(\omega)$. For studying the response of the system it is useful to consider also the q-susceptibility defined as

$$\chi_q(\omega)=\frac{i}{\hbar}\int_0^\infty e^{i\omega t}\langle[q(t),q(0)]\rangle dt. \tag{13}$$

The q-susceptibility is related to the admittance of the system as $Y(\omega)=i\omega\chi_q(\omega)$. Formally, the ϕ-susceptibility corresponds to a ϕ-response under a current perturbation and q-susceptibility corresponds to a q response under a voltage perturbation.

To generalize $\chi(\omega)$ to nonsteady-state cases, we also define a time-dependent susceptibility as

$$\chi(\omega,t)=\frac{i}{\hbar}\int_0^\infty e^{i\omega(t'-t)}\langle[\phi(t'),\phi(t)]\rangle d(t'-t). \tag{14}$$

When relaxation caused by the environment is weak, $\chi(\omega,t)$ changes slowly compared with the internal dynamics of the system and may be considered as a quasistatic quantity. This is the case with a high-Q factor system. In a nonsteady state, the emission and absorption between the system energy levels does not obey the detailed balance condition and $\chi(\omega,t)$ may differ qualitatively from the steady-state susceptibility $\chi(\omega)$ studied in Ref. 14. However, the oscillator-qubit system approaches the thermal equilibrium irrespective of the initial state and, therefore,

$$\lim_{t\to\infty}\chi(\omega,t)=\chi(\omega). \tag{15}$$

In practice, $\chi(\omega,t)\approx\chi(\omega)$ for $t\gtrsim Q/\omega_0$.

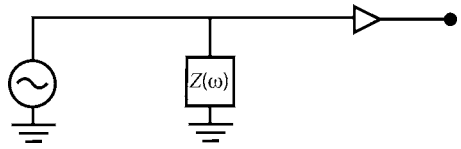

FIG. 4. Realization to carry out transmission impedance measurement of a solid-state quantum circuit. The impedance $Z(\omega)$ represents the coupled oscillator–qubit system. It depends on the quantum state of the system which can be probed by a microwave pulse.

The susceptibility function contains knowledge about the dissipative and reactive response of the system under a weak external perturbation. The susceptibility at a certain moment $\chi(\omega,t_0)$ can be measured by exposing the system to a perturbation acting rapidly compared to the natural relaxation time of the system. In the solid-state context, this could be carried out by connecting the system of interest between input and output transmission lines (Fig. 4) and measuring the transmission of a microwave pulse. Different quantum states of the coupled oscillator and qubit system result in different impedances. By measuring the voltage of the transmitted signal, one can acquire knowledge about the qubit state. The most important requirement for a successful quantum measurement of this kind is that the mixing due to the microwave drive and the relaxation caused by the environment should take much longer than the voltage measurement necessary to identify the state of the system. In practice, the noise originating from the amplifier can be suppressed by using a circulator component. The circulator allows the measurement signal to pass to the amplifier and prevents most of the amplifier noise to perturb the quantum system.

Assuming the drive-induced mixing to be significantly quicker than the environment-induced relaxation, one can calculate a simple estimate for the mixing time. The driving Hamiltonian is assumed to take the form

$$H_d = V_0 q \cos(\omega_d t), \tag{16}$$

where q is the charge operator (12) and V_0 describes the strength of the voltage induced by the microwave field. We assume that the frequency of the measurement signal ω_d coincides closely with an energy difference of two arbitrary energy eigenstates $|i\rangle$ and $|f\rangle$ of the system. An application of the first order time-dependent perturbation theory yields an approximate transition time

$$T_d \approx \frac{2\hbar}{V_0|\langle f|q|i\rangle|} = \frac{\hbar}{eV_0}\sqrt{\frac{Z_b}{R_Q}}\frac{4\sqrt{\pi}}{|\langle f|\hat{p}|i\rangle|}, \tag{17}$$

where $R_Q = h/e^2 \approx 25.6\ \mathrm{k}\Omega$ and $\hat{p} = i(a^\dagger - a)$. After time T_d, the microwave pulse has disturbed the system and lost the information about the initial state in $\chi(\omega_d,t_0)$.

The measurement time T_m is limited from below by the voltage noise of the output signal. The measurement time can be estimated by the signal-to-noise formula

$$S/N = \frac{\Delta V}{\sqrt{S_V T_m^{-1}}}, \tag{18}$$

where S_V is the spectral density of the voltage fluctuations and ΔV is the voltage difference in the signal caused by two differing impedances $Z_1(\omega)$ and $Z_2(\omega)$ of the oscillator. The different impedances $Z_1(\omega)$ and $Z_2(\omega)$ correspond to two different quantum states of the oscillator-qubit system. Supposing that the dominant voltage fluctuations originate from the amplifier, we can write $S_V = 2k_B T_N Z_0$, where T_N is the noise temperature of the amplifier and Z_0 is the characteristic impedance of the transmission line. Setting $S/N = 1$ and solving T_m from Eq. (18), we get

$$T_m = \frac{2k_B T_N Z_0}{(\Delta V)^2} = 4\pi\frac{\hbar k_B T_N}{(e\Delta V)^2}\frac{Z_0}{R_Q}. \tag{19}$$

The transmitted voltage difference between two different states is

$$\Delta V = |V_1 - V_2| = V_0 z, \tag{20}$$

where we defined

$$z \equiv \left|\frac{2(Z_1/Z_0 - Z_2/Z_0)}{(2Z_1/Z_0+1)(2Z_2/Z_0+1)}\right|. \tag{21}$$

The voltage difference is significant when Z_1 and Z_2 are of order Z_0 or one is much larger and the other much smaller than Z_0.

For carrying out a transmission measurement capable of resolving two quantum states, the condition $T_d \gg T_m$ must be fulfilled. Using Eqs. (17) and (19), their ratio is

$$\frac{T_\mathrm{d}}{T_\mathrm{m}} = \frac{\hbar\ V_0 z^2}{k_B T_N Z_0 |\langle f|q|i\rangle|} = \frac{eV_0}{k_B T_N}\frac{\sqrt{Z_b R_Q}}{\sqrt{\pi} Z_0}\frac{z^2}{|\langle f|\hat{p}|i\rangle|}. \tag{22}$$

In the analogous case of current driving,[23] the ratio between the relaxation and measurement times is

$$\frac{T_\mathrm{d}}{T_\mathrm{m}} = \frac{\hbar\ I_0 z^2 Z_0}{k_B T_N |\langle f|\phi|i\rangle|} = \frac{\frac{\hbar}{e} I_0}{k_B T_N}\frac{Z_0}{\sqrt{Z_b R_Q}}\frac{2\sqrt{\pi} z^2}{|\langle f|\hat{x}|i\rangle|}, \tag{23}$$

where $\hat{x} = a^\dagger + a$ and I_0 is the amplitude of the driving field. The matrix element $|\langle f|\hat{p}|i\rangle|$ in Eq. (22) and $|\langle f|\hat{x}|i\rangle|$ in Eq. (23) are of the order of unity in transitions between the lowest energy states. The impedance Z_0 can be matched with Z_1 or Z_2 via a matching circuit, in order to produce an optimal signal. If the requirement $T_d \gg T_m$ is not met, one needs to perform a sequence of measurements to resolve the qubit state.

III. RESULTS

Let us now turn to the impedance $Z(\omega,t) = i\,\omega\chi(\omega,t)$ of the strongly coupled qubit-oscillator system. We characterize the different qubit states by using impedance information and apply this knowledge to the qubit measurements.

We illustrate the dependence of the oscillator impedance on the qubit state by considering an example. In the follow-

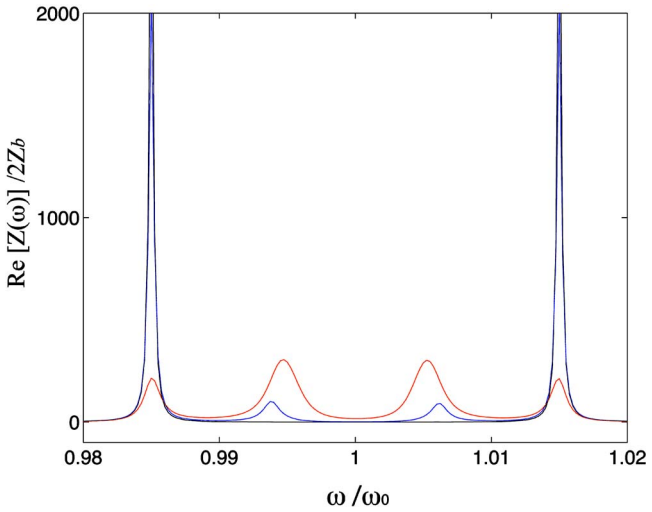

FIG. 5. (Color online) Real part of impedance at $T=\hbar\omega_0/k_b$ (red), $T=\hbar\omega_0/3k_b$ (blue), and $T=\hbar\omega_0/10k_b$ (black).

ing numerical results, we choose the coupling strength $g=0.03\omega_0$ between the oscillator and the qubit and the quality factor $Q=10^4$ of the oscillator. These parameter values are accessible in the solid-state realizations.[5] The ratio between the mixing times γ and κ in the qubit and the oscillator, respectively, is chosen to be $\gamma/\kappa=0.08$. This in agreement with Ref. 5.

The real and imaginary parts of the impedance Z of the system are shown in Figs. 5 and 6 for three different temperatures T of the bath. The coupling between the oscillator and the qubit results in multiple peaks in strong contrast to a single oscillator. Moreover, the impedance of the coupled system is now strongly dependent on temperature. In the low-temperature limit, there are only two peaks in Re$[Z(\omega)]$, corresponding to the vacuum Rabi splitting. They have been experimentally observed recently for example in Ref. 11. The susceptibility is studied as a function of temperature in detail in Ref. 14.

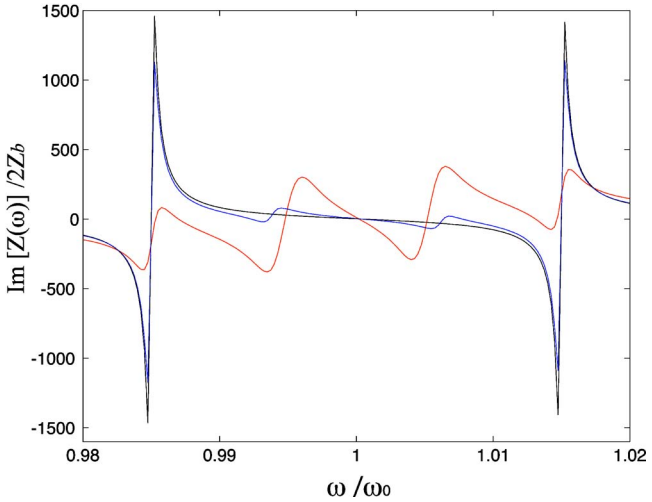

FIG. 6. (Color online) Imaginary part of the equilibrium impedance at $T=\hbar\omega_0/k_b$ (red), $T=\hbar\omega_0/3k_b$ (blue), and $T=\hbar\omega_0/10k_b$ (black).

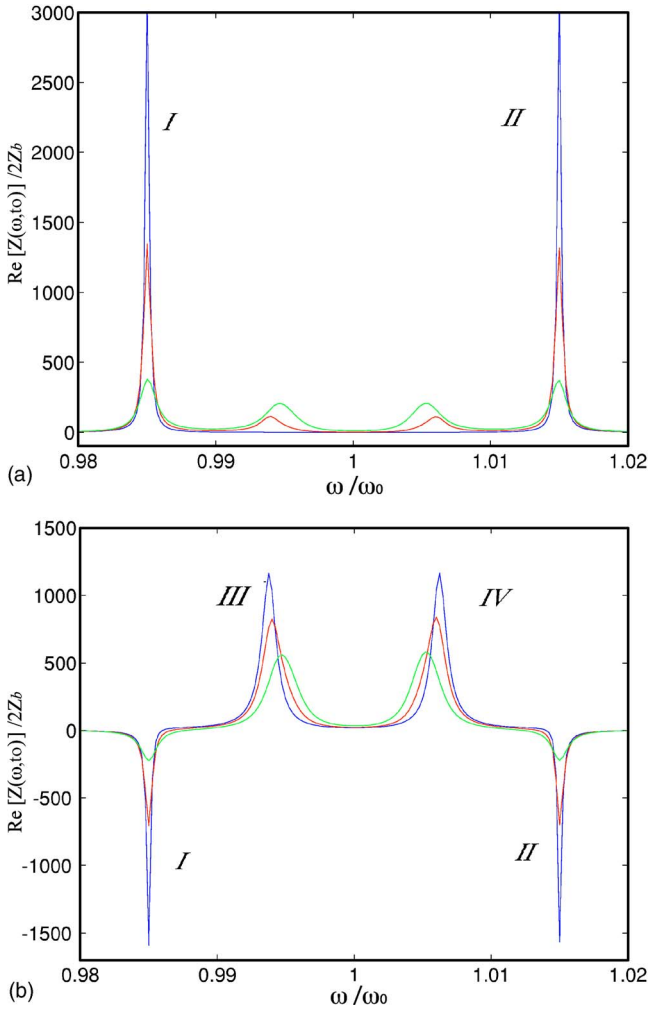

FIG. 7. (Color online) (a) Real part of $Z(\omega,t_0)$ at temperatures $T=\hbar\omega_0/10k_b$ (blue), $T=\hbar\omega_0/2k_b$ (red), and $T=\hbar\omega_0/k_b$ (green). The initial state at $t=t_0$ is prepared so that the oscillator is in the thermal state and the qubit state is up (the lower-energy qubit state). (b) Same as (a) but the initial state is prepared so that the qubit state is down.

When the oscillator-qubit system is not in thermal equilibrium, the susceptibility changes radically (see Fig. 7). The detailed-balance condition, which relates emission and absorption processes, is violated. For example, one can have net emission of energy in some frequencies in addition to the absorption. In those frequencies, the susceptibility takes negative values which lead to negative impedance peaks as in Fig. 7(b). The negative peaks are signs of spontaneous emission of energy and relaxation toward the equilibrium state.

Both sets of impedance curves in Figs. 7(a) and 7(b) contain characteristic peaks which can be utilized to resolve the state of the qubit. At low temperatures, Peaks III and IV are absent in Fig. 7(a). In addition, Peaks I and II are negative in Fig. 7(b). The transitions I–IV are shown in Fig. 8. They correspond to the transitions between the lowest energy states of the coupled system. When the coupling g between the oscillator and the qubit is weak, the lowest-energy states are given in terms of the uncoupled eigenstates as

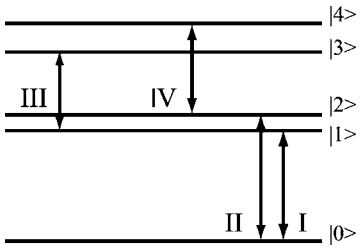

FIG. 8. Transitions corresponding to the four peaks of the low-temperature impedance curves (blue) in Figs. 7(a) and 7(b). Transitions I and II correspond to the vacuum Rabi splitting in (a). The reason that Peaks I and II are negative in Fig. 7(b) is that the initial state is far from equilibrium and spontaneously emits energy.

$$|0\rangle = |n=0\rangle|\uparrow\rangle$$

$$|1\rangle = \frac{1}{\sqrt{2}}(|n=0\rangle|\downarrow\rangle + |n=1\rangle|\uparrow\rangle)$$

$$|2\rangle = \frac{1}{\sqrt{2}}(|n=0\rangle|\downarrow\rangle - |n=1\rangle|\uparrow\rangle)$$

$$|3\rangle = \frac{1}{\sqrt{2}}(|n=1\rangle|\downarrow\rangle + |n=2\rangle|\uparrow\rangle)$$

$$|4\rangle = \frac{1}{\sqrt{2}}(|n=1\rangle|\downarrow\rangle - |n=2\rangle|\uparrow\rangle).$$

The reason for the negative peaks in Fig. 7(b) is that the ground state is unpopulated in the initial state and the system begins to spontaneously increase the ground-state population. All peaks that remain present even in the zero-temperature limit are higher and narrower at lower temperatures. At higher temperatures, new peaks arise. Comparing curves Figs. 7(a) and 7(b), one can also notice that the growth of temperature decreases the differences between the impedance curves corresponding to the different states of the qubit. This phenomenon restricts the accuracy of the qubit measurement based on the impedance difference and puts an upper limit to the measurement temperature to roughly $T \sim \hbar\omega_0/k_b$.

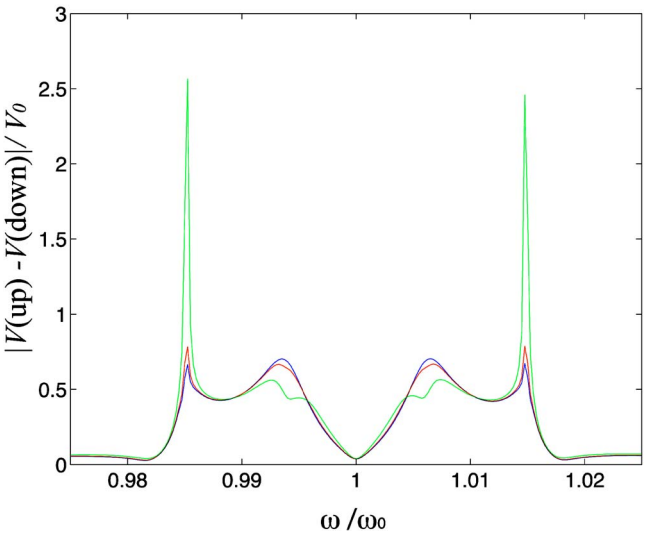

FIG. 10. (Color online) Same as Fig. 9 but with voltage driving. The admittances of the system are calculated from the q-susceptibility (13). As a result, the admittance values accurately agree with impedance values calculated from ϕ-susceptibility and presented in Fig. 7, but in the admittance units $(2Z_b)^{-1}$. In addition, impedances Z_0 and Z_b have been matched to $Z_0/Z_b = 1/500$, which means that the impedance of the system at the peak frequencies are of the same order as that of the transmission line.

In Figs. 9 and 10, we have plotted the difference in the

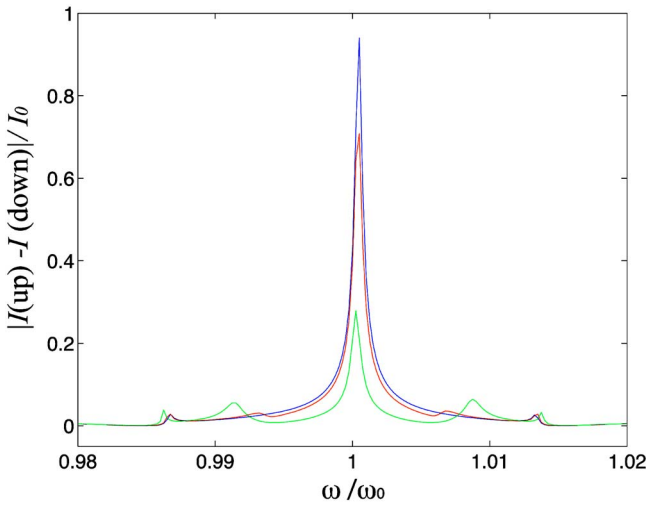

FIG. 9. (Color online) Difference between the transmitted current amplitudes corresponding to the qubit states up and down when the oscillator is in thermal equilibrium at $T = \hbar\omega_0/10k_b$ (blue), $T = \hbar\omega_0/4k_b$ (red), and $T = \hbar\omega_0/2k_b$ (green). The ratio of the impedances Z_b and Z_0 is set to $Z_0/Z_b = 2$.

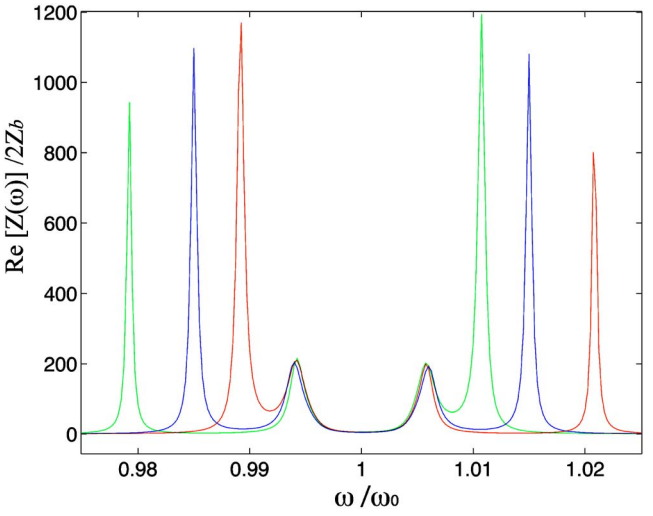

FIG. 11. (Color online) Equilibrium impedance of a resonant and a slightly off-resonant oscillator–qubit system at $T = \hbar\omega_0/2k_b$. The blue curve represents the exactly resonant case, the red curve corresponds to the case $\omega_{qb} = 1.01\ \omega_0$, and the green curve to the case $\omega_{qb} = 0.99\ \omega_0$.

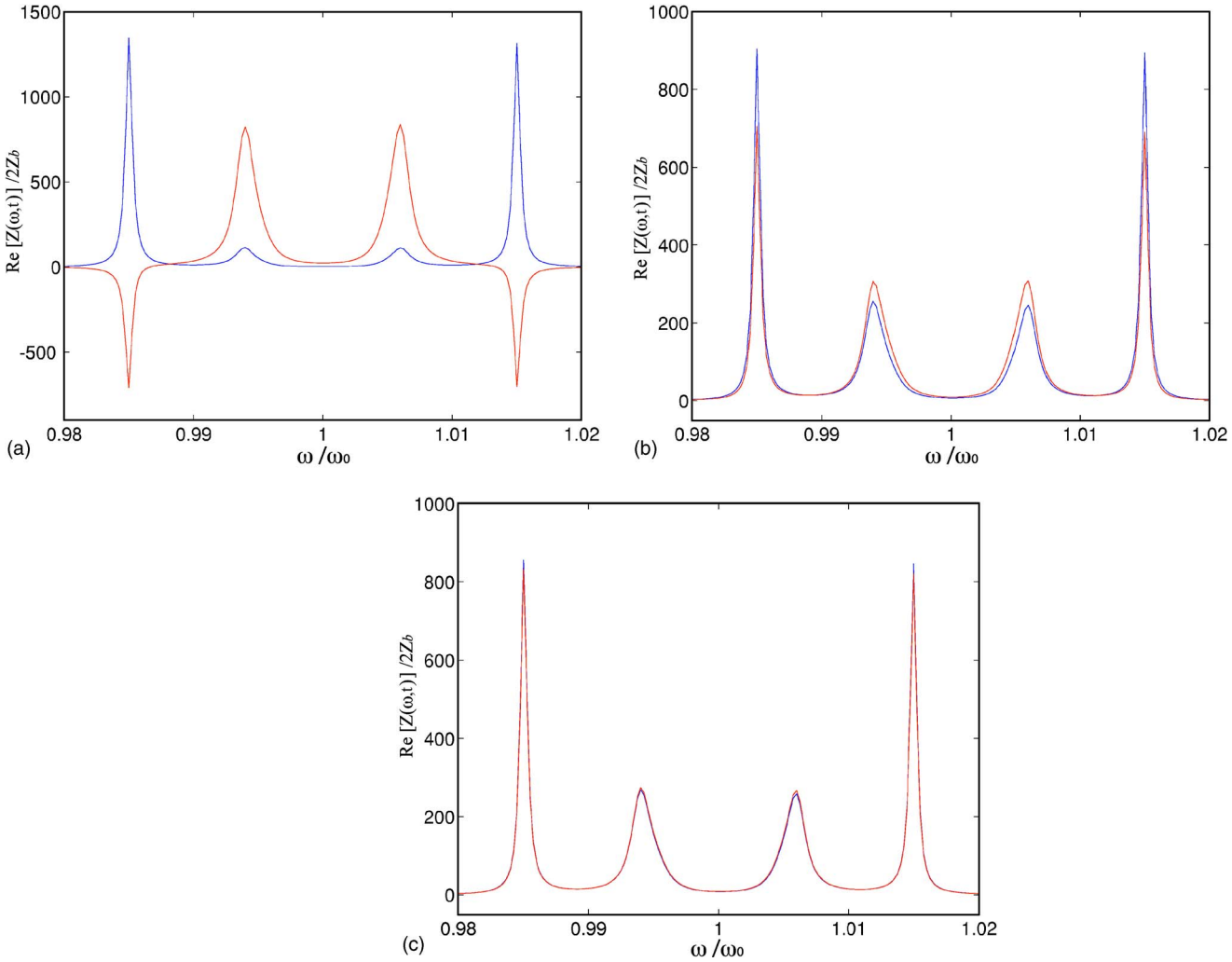

FIG. 12. (Color online) Relaxation of the impedance at $T=\hbar\omega_0/1.8k_b$ as a function of time. The initial state at $t=0$ is prepared so that the oscillator is in the thermal state and the qubit state is up (red line) or down (blue line). The figures correspond to the moments $t=0$, $t=5000\ \omega_0^{-1}$ and $t=10\,000\ \omega_0^{-1}$.

transmitted voltage amplitudes (20), corresponding to the current (ϕ-susceptibility) and voltage (q-susceptibility) driving, respectively. In Fig. 9, the maximum difference does not coincide with the peaks I–IV. This is because the impedance of the system at the peaks is much larger than the characteristic impedance of the transmission line Z_0 and the system effectively decouples from it. However, using an appropriate matching circuit the effective impedance of the system can be varied. Better matching is obtained in Fig. 10, where we consider voltage driven system and the impedance ratio is chosen to $Z_0/Z_b=1/500$. The transmitted voltage amplitude can exceed unity because of the emission associated with Transitions I and II. At temperatures $T=\hbar\omega_0/10k_b$ and $T=\hbar\omega_0/4k_b$, the absolute values of the impedances at Peaks I and II are so high that the system again decouples from the transmission line. That is why the transmitted voltage corresponding to $T=\hbar\omega_0/2k_b$ gives the maximum for this particular impedance matching. The curves are not quite symmetrical with respect to ω_0 because the imaginary part of the impedance is antisymmetric with respect to ω_0.

The impedance of a slightly off-resonant oscillator-qubit system is plotted in Fig. 11. The vacuum Rabi splitting, corresponding to Transitions I and II, is sensitive even to a slight detuning and, thus, the positions of these peaks follow the frequency ω_{qb} of the qubit. On the other hand, the positions of the peaks corresponding to Transitions III and IV follow rather the frequency ω_0 of the oscillator. With small detuning, the height of the impedance peaks is only slightly altered.

As the system relaxes toward the equilibrium state, the impedance settles to the equilibrium pattern. In Fig. 12, we plot the temporal evolution of two nonequilibrium impedances. They correspond to the initial states where the oscillator is in thermal equlibrium and the qubit is prepared either up or down. The susceptibility changes slowly compared to ω_0^{-1} and can be considered as quasistatic. After the time $t \gtrsim Q/\omega_0$, the susceptibilities in both cases are nearly equal, reflecting the uncertainty about the state of the qubit (Fig. 12). When $\gamma \ll \kappa$, the oscillator dissipation yields the dominant time scale for the relaxation of the qubit near resonance.

IV. CONCLUSIONS

In this paper, we discussed the susceptibility and the impedance of a resonant oscillator-qubit system at finite tem-

peratures. We have studied the response of the system in various nonequilibrium states and explored possibilities to apply this phenomenon to determine the state of the qubit. In certain conditions, one can carry out a transmission measurement capable of resolving the qubit state.

Let us estimate the time scales T_d and T_m for an example case with voltage driving. Assume the parameters for the oscillator to be $L=200$ nH and $C=50$ fF. This yields the resonant angular frequency $\omega_0=10$ GHz and characteristic impedance $Z_b=2$ kΩ. Suppose that we are performing the transmission measurement at $T=\hbar\omega_0/(4k_b)=20$ mK or $T=\hbar\omega_0/(2k_b)=40$ mK, corresponding to the red and green curves in Fig. 10. We further assume that the amplifier is impedance matched such that the amplifier looks to the sample as an impedance $Z_0=Z_b/500$. This can be accomplished via a transformer circuit. Now taking $eV_0=0.03\hbar\omega_0=0.2\mu$V and $T_N=5\hbar\omega_0/k_b=400$ mK, we get the measuring time $T_m=17/\omega_0=1.7$ ns, and the relaxation time $T_d=93/\omega_0=9.3$ ns. Thus, it should be possible to carry out the qubit measurement before the qubit relaxes. These numbers were calculated by assuming $z=0.8$ and $|\langle f|\hat{p}|i\rangle|=1/\sqrt{2}$. The ratio T_d/T_m can be further improved for voltage driving if Z_b can be made larger, Z_0 smaller, or if the noise temperature T_N can be decreased. Note that the estimate (17) is a pessimistic one: The off-resonant mixing time is longer than when the driving frequency corresponds exactly to the position of the impedance peaks.

The above analysis was done by treating the transmitted signal classically. To examine the possibility of a single-shot measurement, the proper quantitative analysis would require the quantization of the electromagnetic field in the transmission line and solving the full quantum-mechanical dynamics in detail. This analysis is beyond the scope of this paper. In any case, the above analysis demonstrates that the thermal noise does not prevent the possibility of a successful single-shot measurement.

ACKNOWLEDGMENTS

We thank Mika Sillanpää, Pertti Hakonen, and Göran Johansson for valuable discussions. One of the authors (T. T. H.) acknowledges the financial support by the Academy of Finland and the NCCR Nanoscience.

*Correspondence to teemuo@boojum.hut.fi

[1] V. B. Braginsky and F. Ya. Khalili, *Quantum Measurement* (Cambridge University Press, Cambridge, U. K., 1992).
[2] D. V. Averin, in *Quantum Noise in Mesoscopic Physics*, NATO Science Series II Vol. 97, edited by Yu. V. Nazarov (Kluwer, Dordrecht, 2003), p. 229 [cond-mat/0301524].
[3] A. N. Korotkov and D. V. Averin, Phys. Rev. B **64**, 165310 (2001).
[4] A. A. Clerk, S. M. Girvin, and A. D. Stone, Phys. Rev. B **67**, 165324 (2003).
[5] A. Blais *et al.*, Phys. Rev. A **69**, 062320 (2004).
[6] D. I. Schuster *et al.*, cond-mat/0408367.
[7] S. M. Girvin *et al.*, *Proceedings of Les Houches Summer School, Session LXXIX, Quantum Entanglement and Information Processing* (2003) [cond-mat/0310670].
[8] E. Il'ichev *et al.*, Low Temp. Phys. **30**, 620 (2004).
[9] Yu. Makhlin, G. Schön, and A. Shnirman, Nature (London) **431**, 138 (2004).
[10] I. Chiorescu *et al.*, Nature (London) **431**, 159 (2004).
[11] A. Wallraff *et al.*, Nature (London) **431**, 162 (2004).
[12] A. Yu. Smirnov, Phys. Rev. B **68**, 134514 (2003).
[13] H. Xu *et al.*, Phys. Rev. Lett. **94**, 027003 (2005).
[14] I. Rau, G. Johansson, and A. Shnirman, Phys. Rev. B **70**, 054521 (2004).
[15] A. O. Caldeira and A. J. Leggett, Phys. Rev. Lett. **46**, 211 (1981).
[16] R. P. Feynman and F. L. Vernon, Ann. Phys. (N.Y.) **24**, 118 (1963).
[17] J. Rammer, *Quantum Transport Theory* (HarperCollins, New York, 1998).
[18] A. Käck, G. Wendin, and G. Johansson, Phys. Rev. B **67**, 035301 (2003).
[19] H. Schoeller and G. Schön, Phys. Rev. B **50**, 18436 (1994).
[20] H. J. Carmichael, *Statistical Methods in Quantum Optics 1: Master Equations and Fokker-Planck Equations* (Springer, Berlin, 1999).
[21] C. Cohen-Tannoudji, J. Dupont-Roc, and G. Grynberg, *Atom-Photon Interactions* (Wiley, New York, 1992).
[22] Michel H. Devoret, in *Les Houches, Session LXIII, 1995* (Elsevier Science, Amsterdam, 1997), p. 351.
[23] The case of voltage driving is realized if the inductor L and capacitor C are in series, and of current driving for their parallel configuration. In the previous case, one is interested in the q-susceptibility, and in the latter case, in the ϕ-susceptibility. The results for the two are qualitatively similar, in the former case the admittance taking the role of the impedance.